Through the Soil Long Range Wireless Power Transfer for Agricultural IoT Networks

Brandon T. Nieman[1], *Student Member*, Christopher S. Johnson[2], *Student Member*,
Matthew Pearce[1], *Member*, Tyler Marcrum[1], *Student Member*, M. Caleb Thorne[2], Carter Ashby[2],
C. W. Van Neste[2], *Senior Member*,
[1]Center for Energy Systems Research
[2]Electrical and Computer Engineering Department
Tennessee Technological University
Cookeville, TN, 38505
cvanneste@tntech.edu

***Abstract*—Increasing the spatial and temporal density of data using networked sensors, known as the Internet of Things (IoT), can lead to enhanced productivity and cost savings in a host of industries. Where applications involve large outdoor expanses, such as farming, oil and gas, or defense, large regions of unelectrified land could yield significant benefits if instrumented with a high density of IoT systems. The major limitation of expanding IoT networks in such applications stems from the challenge of delivering power to each sensing device. Batteries, generators, and renewable sources have predominately been used to address the challenge, but these solutions require constant maintenance or are sensitive to environmental factors. This work presents a novel approach where conduction currents through soil are utilized for the wireless powering of sensor networks, initial investigation is within an 0.8-ha (2-acre) area. The technique is not line-of-sight, powers all devices simultaneously through near-field mechanics, and has the ability to be minimally invasive to the working environment. A theory of operation is presented and the technique is experimentally demonstrated in an agricultural setting. Scaling and transfer parameters are discussed.**

***Keywords*—Wireless power transfer, Through the Soil, Long Range, conduction**

I. Introduction

Decision making based on real-time/measured data is critically important to boosting revenue/productivity in many industries. Sensor installation throughout the industrial process plays a fundamental role in these tools. The number of sensors that can be installed is limited by two primary factors: (1) the cost (including installation/maintenance) of the sensor and (2) the power source used by the sensor. Recent advances in electronics/manufacturing have effectively solved many of the sensor cost challenges. However, there are few low-maintenance/low-profile solutions to delivering power to a multitude of sensor systems. Difficulties in power delivery are only amplified when applications require monitoring in remote and expansive outdoor environments. This is specifically challenging in industries such as farming, where large tracts of land are usually far from any electrical supply. Weather dependent sources such as photovoltaics, wind turbines, etc., or the continual replacement of batteries are the only real solution to this problem, all of which do not support IoT scaling. These conventional power methods can be intrusive to the working environment as devices can become entangled in or damaged by equipment/livestock/wildlife. Motorized equipment (such as tractors) must maneuver around solar and wind charging solutions, and as crops, trees, or vegetation mature, they may become completely overshadowed and/or entwined. Thus, contemporary power solutions make the installation of sensing tools time consuming, costly, and in many cases, impractical as the number of sensors are increased.

These electric power supply limitations have led to WPT research that encompasses both near-field and far-field techniques. Radio Frequency (RF) energy harvesting [1] or robotic drones [2], [3] have both been developed for transferring electric power to soil sensors [4]–[10]. RF energy harvesting requires the rectification of space-wave signals that do not penetrate far beneath the soil surface and require a substantial time to collect enough energy to perform a function. Drones, either land- or air- based, are generally equipped with a magnetic coupling WPT system that transfers energy to sensors when the drone is positioned directly over the sensor's receiver. A drone solution adds navigation complexities, high power consumption for locomotion, high operating/maintenance expenses, and limited spatial coverage unless multiple drones are used – compounding all factors. Neither of these solutions supports wide area IoT scaling, with both suffering from efficiency losses when sensors are buried below 15 cm – as bulk soil is conductive, causing high attenuation of an electromagnetic wave's magnetic component at the frequencies used.

Manuscript received Month xx, 2xxx; revised Month xx, xxxx; accepted Month x, xxxx. This work was supported in part by the National Science Foundation under Award Nos. 1841469 and 2226612.

C.W. Van Neste, Tennessee Tech University, Cookeville, 38501, USA (cvanneste@tntech.edu).

Long range forms of WPT (LR-WPT) have also been investigated. These rely on the transmission of focused electromagnetic (EM) space-waves. In this category, there are two predominant LR-WPT technologies in use, laser power beaming and RF microwave power transfer (MPT) [11]–[14]. Both techniques use far-field electromagnetic waves to transfer power. Literature has shown that MPT is more reliable for transmission between fixed installations [11]. Zhu [12] gives a side-by-side summary of present MPT endeavors. These systems either exhibit very low efficiency or have short transmission distances [14], [15]. While some companies are commercializing laser power beaming and MPT based systems, they are in the very early stages of development with limited prototypes demonstrated [16], [17]. All such systems are line-of-sight dependent and require large, complex rectenna arrays to lower the power density during transmission to improve safety (as the wavelengths used are typically limited to 1W or lower exposure limits). Neither of these LR-WPT systems would make good candidates for powering expansive IoT networks.

More obscure in present literature is the non-line-of-sight approaches where energy is transferred along the surface of the earth with a ground wave [18], [19]. Viziv Technologies is a company that claims to be working on ground wave propagation for power transfer [20], [21]. These systems utilize tall above-ground antenna structures to induce charge oscillations at the surface. To date, no physically realized experiments have been publicly demonstrated by Viziv and based on the data presented in the limited literature, the given distributed electric field intensities are much too weak for long range wireless power transfer [20].

It can be concluded that there currently exists no other techniques beyond line-of-sight far-field radiation that has demonstrated LR-WPT. This manuscript presents a first of its kind WPT concept that utilizes conduction currents "through the soil" (TTS) to transfer power to surrounding devices. The presented system is not line of sight dependent and is observed to be robust in the limited locations tested[22]. The geometry of the TTS system is similar to a water well, offering a possible way to integrate this LR-WPT technique into existing farming infrastructure at very little cost to the user. The theory of operation will be expanded from earlier studies by the authors. A horizontal receiver geometry will be presented and an agricultural case-study using 4 IoT devices without batteries will be shown as proof of concept. A section on range and efficiency will explore possible methods for future improvements to the system.

II. Theory and Derivations

This section presents methods used to investigate the dynamics of the TTS system. First, a lumped circuit model is developed to identify the parameters that affect efficiency. Next, a concept based on electromagnetic field theory is presented for determining the received voltage distribution in the soil as a function of radial distance around the transmitter. This same theory also provides an expression for the soil's impedance, linking the source current to the received voltage at a distance.

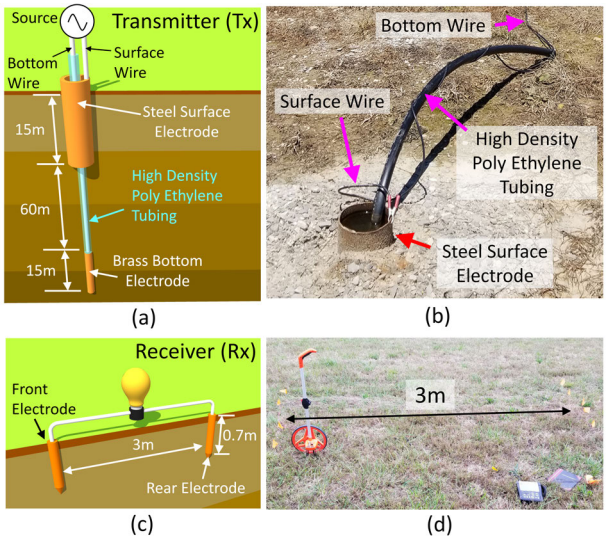

Fig. 1. (a) Diagram of the Transmitter's (Tx) topology showing in connection to the soil. (b) Annotated photograph of the Tx. (c) Diagram of the Receiver's (Rx) topology in connection to the soil. (d) Photograph of the Rx with electrodes marked with flags.

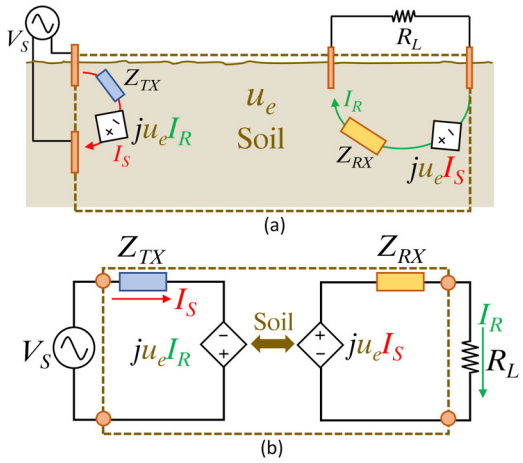

Fig. 2. Coupled circuit model for TTS system.

The theory for the potential distribution is experimentally verified over 0.8-ha in an adjacent hay field. The theory is then combined with the lumped circuit model to arrive at an approximate equation for the system's efficiency with parameters that will serve as metrics for future improvements to the system.

A. Geometry and Circuit Model

The TTS transmitter (Tx) utilized a minimum of two conductors (defined as electrodes) in direct contact with the soil, where one electrode resided at the soil surface and the other resided at a vertical distance below the surface (defined as a vertical geometry). The top electrode was formed from a well casing that was installed around the bore-hole of the Tx. The well casing was made of low carbon steel that was approximately 15m long. The bottom electrode was a 15m section of brass tubing (50mm in diameter), located 75m

below the surface. The brass tubing was connected to a High Density Poly Ethylene (HDPE) tubing of the same diameter that ran from the brass to the surface. A 12 gauge insulated wire was fastened to the inside of the brass tubing at the bottom, and ran to the surface on the inside of the HDPE. Thus, the wire allowed an electrical connection to the bottom electrode from the surface, with the wiring being isolated from the surrounding soil via the HDPE tubing.

The receiver (Rx) for this work was constructed using a horizontal geometry, where both electrodes (0.7m long) resided at the surface. This is shown in Fig. 1 where an annotated illustration of the geometry is depicted next to a photograph of the experimental system. The horizontal geometry of the Rx was chosen for the ease of deployment and measurement. Future investigations will explore vertical topologies for the Rx, whose placement will become more permanent. A basic schematic of the system and its corresponding circuit is shown in Fig. 2(a) with orange bars indicating the electrodes.

Due to soil strata layers being mostly horizontal, current injected into the ground will follow strata layers of lower resistivity and not spread (or fringe) as far within the surrounding soil medium [23]. This makes horizontal Tx geometries more prone to changes in conductivity due to weather and less effective at transmitting energy over the surrounding area. A vertical Tx structure exhibits greater current fringing since moving charge must traverse all strata layers (regardless of their variations in conductivity). The vertical geometry is therefore a better design choice for the Tx. For the Rx, the only geometric constraint is that its electrodes must reside at different equipotential lines created by the Tx in order for a voltage to be received.

The energy exchange between the Tx and Rx was modeled as a pair of coupled circuits (Fig. 2(b)). This model is only slightly different from the current controlled voltage source model presented in [24]. The difference between the two models is that the coupled circuit allows impedance variations at the Rx to be seen by the Tx, which is expected to occur once the resistive components of Z_{TX} and Z_{RX} are made small. The transfer efficiency (η) of the system can be approximated using this model. Applying loop analysis produces two circuit equations

$$-V_S + Z_{Tx}I_S - j(u_e)I_R = 0 \tag{1}$$

$$-j(u_e)I_S + Z_{Rx}I_R + R_L I_R = 0 \tag{2}$$

The direction of the coupling is chosen such that current flowing in the received circuit will reduce the reactive component in the supply circuit - similar to a transformer. The received voltage (V_R) takes the form:

$$V_R = ju_eI_s = \Phi(r) \tag{3}$$

where u_e is a lumped "earth impedance" that is dependent on the distance (r) from the Tx. The potential difference in the soil, ($\Phi(r)$), is derived in the next subsection.

Using (1) and (2), the source current (I_S) and received current (I_R) are solved for yielding:

$$I_S = \frac{(R_L + Z_{Rx})V_S}{Z_{Tx}(R_L + Z_{Rx}) + (u_e)^2} \tag{4}$$

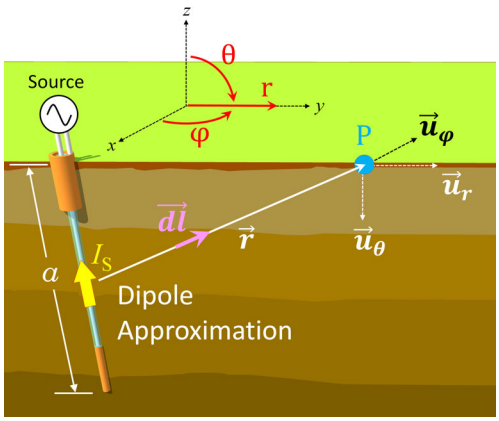

Fig. 3. Dipole approximation used for deriving the potential distribution around the TTS transmitter. Point P corresponds to the measurement location.

$$I_R = \frac{j(u_e)V_S}{Z_{Tx}(R_L + Z_{Rx}) + (u_e)^2} \tag{5}$$

Eq. (5) will be used in the next section to validate the model. The input power (P_{IN}) and load power (P_L) are,

$$P_{IN} = V_S I_S = \frac{(R_L + Z_{Rx})(V_S)^2}{Z_{Tx}(R_L + Z_{Rx}) + (u_e)^2} \tag{6}$$

$$P_L = R_L(I_R)^2 = \frac{(u_e)^2(V_S)^2 R_L}{(Z_{Tx}(R_L + Z_{Rx}) + (u_e)^2)^2} \tag{7}$$

Dividing (7) by (6) gives the power transfer efficiency (η)

$$\eta = \frac{P_L}{P_{IN}} = \frac{R_L u_e^2}{(Z_{Tx}(Z_{Rx} + R_L) + (u_e)^2)(R_L + Z_{Rx})} \tag{8}$$

B. Deriving the Potential Distribution

To determine u_e, the voltage distribution around the Tx must be derived with respect to the radial distance r. The complex network of resistances, capacitances, and inductances that would be needed to model the soil are difficult to approximate and challenging to measure. Fortunately, the Tx geometry is similar to, and can be approximated as, an electric dipole. By solving for the electric field of this dipole (modeling the medium as a lossy dielectric), it should be possible to integrate the electric field radially to find the potential distribution along the ground. The usefulness of the dipole approximation is that it links source current injected into the Tx to the voltage distribution, mitigating the need of developing a complex impedance model of the soil.

Referring to Fig. 3 for the time varying electric dipole approximation, the perceived separation distance (d) of the point charges is first modified from a conventional dipole to be the circumference of a toroidal path the current would traverse. (d) becomes,

$$d = 2\pi a \tag{9}$$

where a is the physical separation distance between the electrodes in the soil as shown in Fig. 3. Taking the vector

potential ($\overrightarrow{A}$) expressed in the frequency domain, the magnetic field intensity is

$$\overrightarrow{A}_{zs} = \frac{\mu I_S d}{4\pi r} e^{-j\beta r} \left[\overrightarrow{u}_z\right]$$

$$\overrightarrow{H} = \nabla \times \overrightarrow{A}$$

$$\overrightarrow{H} = \frac{I_S d}{4\pi} \left(\sin\theta\right) e^{-j(\beta r)} \left[\frac{j\beta}{r} + \frac{1}{r^2}\right] \left[\overrightarrow{u}_\varphi\right] \tag{10}$$

where I_S is the source current driving the Tx, β is the phase constant, $\overrightarrow{r}$ is the distance vector from the center of the electrodes to the point where the field is being measured, and $[\overrightarrow{u}_\varphi]$ is the unit vector in the φ-direction. The electric field is found by applying Ampere's law

$$\nabla \times \overrightarrow{H} = \varepsilon \frac{\partial \overrightarrow{E}}{\partial t} + \overrightarrow{J}$$

$$= \left(\sigma + j\omega\varepsilon\right) \overrightarrow{E} \tag{11}$$

where (σ) is the soil conductivity and ω is the angular frequency. Solving (11) for $\overrightarrow{E}$ yields the electric field intensity as a function of the radial distance r

$$\overrightarrow{E} = \frac{2 I_S d}{4\pi\left(\sigma + j\omega\varepsilon\right)} \cos\theta \left[\frac{j\beta}{r^2} + \frac{1}{r^3}\right] e^{-j(\beta r)} \left[\overrightarrow{u}_r\right]$$
$$+ \frac{I_S d}{4\pi\left(\sigma + j\omega\varepsilon\right)} \sin\theta \left[\frac{\beta^2}{r} - \frac{j\beta}{r^2} + \frac{1}{r^3}\right] e^{-j(\beta r)} \left[\overrightarrow{u}_\theta\right] \tag{12}$$

The field distribution of (12) has three main operational regions [25]: the static region proportional to $1/r^3$, the induction region proportional to $1/r^2$, and the far region (or radiation region) proportional to $1/r$. Both the static and induction regions are related to the near-field of the electric dipole.

In practice, it is the voltage produced within the soil that can be directly measured. The potential difference (Φ) is given by

$$\Phi = -\int \overrightarrow{E} \cdot \overrightarrow{dl} \tag{13}$$

where $\overrightarrow{dl} = dr\left[\overrightarrow{u}_r\right] + rd\theta\left[\overrightarrow{u}_\theta\right] + r\sin\theta d\varphi\left[\overrightarrow{u}_\varphi\right]$. The integral of the dot product produces

$$\Phi(r) = \frac{I_S d\left(\sigma - j\omega\varepsilon\right)}{4\pi\left(\sigma^2 + \left(\omega\varepsilon\right)^2\right)} \cos\theta \left[\frac{2e^{-j(\beta r)}}{r^2} + \beta^2 e^{-j(\beta r)}\right.$$
$$\left. - \beta^2 Ei\left(-j\beta r\right)\right] \tag{14}$$

The exponential integral $Ei\left(-j\beta r\right)$ can be expanded using integration by parts

$$Ei\left(x\right) = -\frac{e^{-x}}{x} - \frac{e^{-x}}{x^2} - 2\int \frac{e^{-x}}{x^3} dx... \tag{15}$$

Since r^3 was the highest order term in (12), it is expected that the contributing potential should have a maximum order of r^2 due to integration; taking note that the integration reduces the order such that the radiation region of the potential becomes a constant, the induction region becomes $1/r$, and the static region becomes $1/r^2$. All higher order terms beyond the second order can be neglected. Substituting (15) into (14) and rearranging gives

$$\Phi(r) = \frac{I_S d\cos\theta}{4\pi\left(\sigma^2 + \left(\omega\varepsilon\right)^2\right)} e^{-j(\beta r)} \left[\left(\sigma\beta^2 + \frac{\omega\varepsilon\beta}{r} + \frac{\sigma}{r^2}\right)\right.$$
$$\left. + j\left(-\omega\varepsilon\beta^2 - \frac{\sigma\beta}{r} - \frac{\omega\varepsilon}{r^2}\right)\right] \tag{16}$$

In (16), the terms $\sigma\beta^2$ and $-\omega\varepsilon\beta^2$ are related to the radiation region and are negligible at near-field distances. Similarly, $e^{-j(\beta r)}$ is approximately 1. (16) can be rewritten as

$$\Phi(r) = \frac{I_S d\cos\theta}{4\pi\left(\sigma^2 + \left(\omega\varepsilon\right)^2\right)} \left[\left(\frac{\omega\varepsilon\beta}{r} + \frac{\sigma}{r^2}\right)\right.$$
$$\left. - j\left(\frac{\sigma\beta}{r} + \frac{\omega\varepsilon}{r^2}\right)\right] \tag{17}$$

In order for the soil to appear like a conductor, the Tx should be driven within the SLF to VLF frequency band (30Hz to 30kHz). In this frequency range, $\omega\varepsilon$ becomes small, making (17) more a function of soil conductivity

$$\Phi(r) \propto \left(\frac{1}{\sigma r^2} - j\frac{\beta}{\sigma r}\right) \tag{18}$$

The real term in (18) is extraneous since conductivity in the static region ($1/r^2$), is significantly dependent on temporal charge relaxations [26], not spatial distribution. We can therefore neglect the real component of (17), taking only the imaginary

$$\Im\mathrm{m}\{\Phi(r)\} = \Im\mathrm{m}\left\{\frac{I_S d\cos\theta}{4\pi\left(\sigma^2 + \left(\omega\varepsilon\right)^2\right)} \left[\left(\frac{\omega\varepsilon\beta}{r} + \frac{\sigma}{r^2}\right)\right.\right.$$
$$\left.\left. - j\left(\frac{\sigma\beta}{r} + \frac{\omega\varepsilon}{r^2}\right)\right]\right\}$$

$$\Phi(r) = -\frac{I_S d}{4\pi\left(\sigma^2 + \left(\omega\varepsilon\right)^2\right)} \left(\frac{\sigma\beta}{(r)} + \frac{\omega\varepsilon}{(r)^2}\right) \tag{19}$$

Eq.(19) allows one to calculate the approximate voltage radially from the Tx. It should be noted that the electric field is polarized in the $\overrightarrow{u}_\theta$-direction and thus the $\cos\theta$ term is typically one. Additionally, since the assumption of this derivation is that the soil acts as a good conductor, the electric field at the soil/air interface must be vertical due to continuity, which again assumes an electric field in the $\overrightarrow{u}_\theta$-direction and a $\cos\theta$ term equal to one.

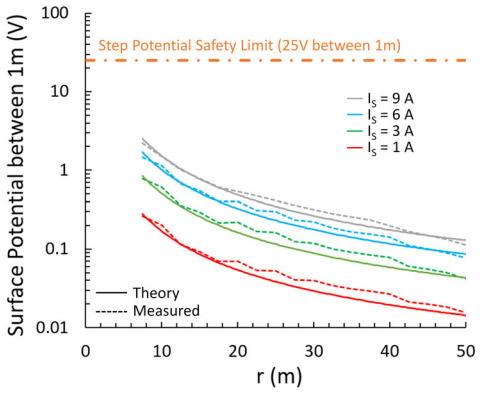

Fig. 4. Experimentally measured data (**Dashed Trace**), vs calculated values using theoretical model (**Solid Trace**) for various peak drive currents. The orange dash-dot line shows the setup potential safety limit for the system.

Taking (19) and dividing it by the source current (I_S) produces the equation for u_e, that can be inserted into (5) and (8)

$$u_e = -\frac{d}{4\pi\left(\sigma^2 + (\omega\varepsilon)^2\right)}\left(\frac{\sigma\beta}{r} + \frac{\omega\varepsilon}{r^2}\right) \tag{20}$$

C. Theoretical and Circuit Validation

To validate (19), and with it (20), the Tx was driven at various currents (I_S) from 1A to 9A and radial measurements were taken using steel stakes as the Rx electrodes and a Tektronix THS3024 battery powered oscilloscope to quickly measure voltages between two points at the soil surface. The potential differences were measured every 2.5m, within a 50m radius around the Tx. The data was then normalized to a 1m spacing to compare its value with the safety limit of 25V over 1m [27].

The theoretical response was calculated from (19) using the soil Φ-parameters given in Table I. Fig. 4 shows the measured and theoretical traces plotted side by side. The theory matches the experimental data well, with slight variations due to the simplifying assumption that the soil is homogeneous, whereas in reality, soil is a heterogeneous medium. The results of Fig. 4 indicate (19) can be readily used to predict the potential difference over the area.

With u_e verified, the accuracy of the circuit model in Fig. 2 was tested. The electrode spacing was fixed at 1m, and both front and rear electrodes were moved together away from the Tx at 1m intervals (see Fig. inset for illustrated layout). This is plotted in Fig. 5(a). Using the measured Tx and Rx parameters in Table I, with a drive voltage that produced 6A in the Tx, the short-circuit Rx current was calculated from (5) and plotted in the figure. The circuit model approximately follows the experimental data. Next, the effects of the Rx electrode spacing were tested. The front electrode was kept stationary at 10m from the Tx while the rear electrode was moved backwards in 1m intervals. Both the measured open-circuit voltage and short-circuit current are plotted in Fig. 5(b). The received voltage at the Rx electrodes was found to be the

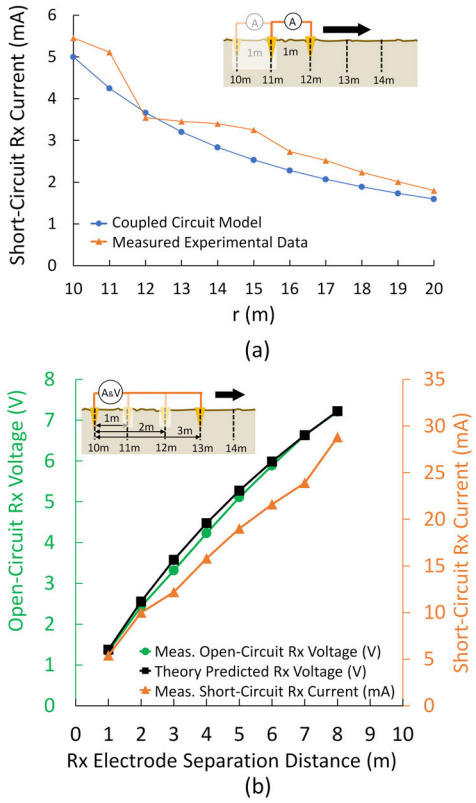

Fig. 5. (a) Plot of the short-circuit Rx current predicted in the coupled circuit model versus the measured short-circuit Rx current between electrodes spaced 1m and moved away from the Tx, starting at 10m and ending at 20m (see inset). (b) Experimental data showing the measured voltage of the Rx as the electrode separation is increased compared with what is predicted by the theory using (19). Note that the front electrode was placed 10m from the Tx and the rear electrode was moved in 1m increments away from the Tx.

sum of the potential between the electrodes, allowing one to utilize (19) to estimate the value of received voltage based on the Rx electrode separation at any distance away from the Tx.

From Fig. 5(b), it can be seen that as the electrodes are moved further apart, the maximum received power increases. However, the non-linear distribution of the potential decreases with distance (as shown in Fig. 4), putting a limit on the received power as the Rx is made significantly long (aka the power does not continue to raise indefinitely as the Rx electrode separation is made larger). Long Rx geometries are also seldom feasible. For this study the Rx electrodes were kept at 3m, as this gave the minimum received power to operate the sensors while being at least a third smaller than the closest tested distance from the Tx (10m). A unique feature of this power transmission technique is that as the injected Tx current was raised, the sensors could either support a larger load, or they could be moved farther away from the Tx. At 9A, it was possible to power the sensor modules at approximately 20m from the Tx.

D. Simulation

With the theoretical and circuit model validated, it is important to develop a simulation that matches the proper conditions

TABLE I
SOIL MODEL PARAMETERS

Φ-Parameter	Value	Circuit-Parameter	Value
f	60 Hz	Z_{TX}	27 Ω
σ	0.4 mS/m	Z_{RX}	246 Ω
ε_r	4	R_L	0.1 Ω
μ_r	1	V_S	162 V_{Peak}

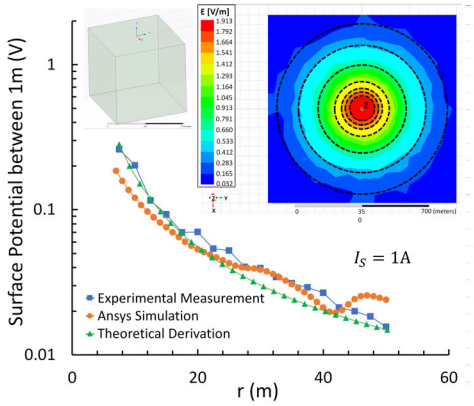

Fig. 6. **(a)** Ansys Maxwell simulation of TTS Tx for a 1A injection and the accompanying E-field distribution over the surface of the earth. Dashed circles added to highlight the equipotential lines. **(b)** Comparison of the surface potential using the Ansys simulation vs the theoretical derivation, vs the experimental measurement driving the Tx at 1A.

of the TTS system. For this work, Ansys Maxwell was used. Future work will utilize this model for investigating better electrode designs, whereas the theoretical/circuit model can be used for quick calculations to determine Tx drive magnitudes and maximum distances sensors can be placed based on the Rx electrode spacing.

Fig. 6(a) shows the results from the Ansys simulation for a 1A drive current into the Tx. A 1km, homogeneous cube was modeled as the earth using the same values in Table I. The viewpoint in the figure is top down, depicting the electric field (E-field) at the surface of the cube in the xy-plane and the equipotential regions, exemplified with dashed concentric rings. For the Rx to develop a voltage, the front and rear Rx electrodes must be located on different equipotential lines.

The simulated values of the E-field were extracted from the simulation and integrated with the distance to obtain the surface potential. The simulated values of the surface potential were then plotted next to the theoretical and experimental values for comparison (Fig. 6(b)). It can be seen that both the Ansys model and the theoretical derivation are all in close approximation to the experimental measurements taken in the adjacent agriculture field.

III. POWER TRANSFER FOR IOT APPLICATIONS

A small IoT network of commercial agricultural sensors were used to demonstrate the systems ability to wirelessly transfer power *without* batteries or large electric storage elements. Do note that a 1mF capacitor (Fig. 7(b)) was used for DC filtering and did provide energy for the 0.2W bursts the sensor required when transmitting data. The sensors were all

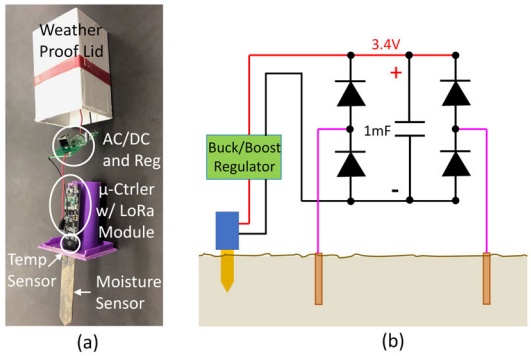

Fig. 7. **(a)** Photograph of IoT sensor module showing various components. **(b)** Schematic of the rectifier electronics used to convert the AC conduction currents in the soil to DC, powering the sensor module. The module required 3.4V and 10mA to operate (60mA to transmit data).

powered simultaneously within a radius tested between 10m to 20m around the Tx.

The sensor modules are shown in Fig. 7 and include an integrated moisture and temperature sensor. The microcontroller (μ-ctrl) on each module is an ATMega32u4 with a LoRa communications IC (integrated circuit).

Fig. 7(a) is an annotated photograph of the sensor module identifying the various components. Fig. 7(b) is a schematic that shows the basic rectification electronics used in the module. A full bridge rectifier, connected to the Rx electrodes, converted the conduction currents created by the Tx into a DC voltage that was then regulated with a buck/boost converter. When the sensors were powered, soil moisture and temperature data was collected and transmitted via conventional space waves at 900MHz, to a receiving ESP32 at the base station. The ESP32 was only used as a microcontroller, with an attached LoRa module to accept the 900MHz protocol. The ESP32 would then relay the data through serial to a computer for storage and post-processing. Each sensor was waterproofed for long-term measurement studies via a box with a rubberized coating. The sensors were calibrated prior to their deployment.

Fig. 8(a) is a photograph of the experimental system's layout with deployed sensors. Illustrations of the Tx and horizontal Rx are inset in the photo for additional clarity. The data was collected for 1 minute each hour, continuously over a 7-day period. Fig. 8(b) is a plot of the soil data collected from the four sensors that formed the IoT network.

IV. DISCUSSION ON IMPROVEMENTS IN RANGE AND TRANSFER EFFICIENCY

Equations (8) and (20) predict that the efficiency of the TTS system is strongly dependent on the impedance of the Tx and Rx. Impedance data of the Tx has been collected for several years at the Tennessee location, with the first study on the technique being conducted in Alberta Canada in 2015 [23]. Fig. 9 is a plot of the impedance modulus variations over different seasons, weather types, and locations. In the figure, *Fair* weather is defined as either full or partial sun, the other weather descriptors are self explanatory. It can be seen that the impedance of the Tx has a low-Z region and a high-Z region. The high-Z corresponds to a cross-over point where

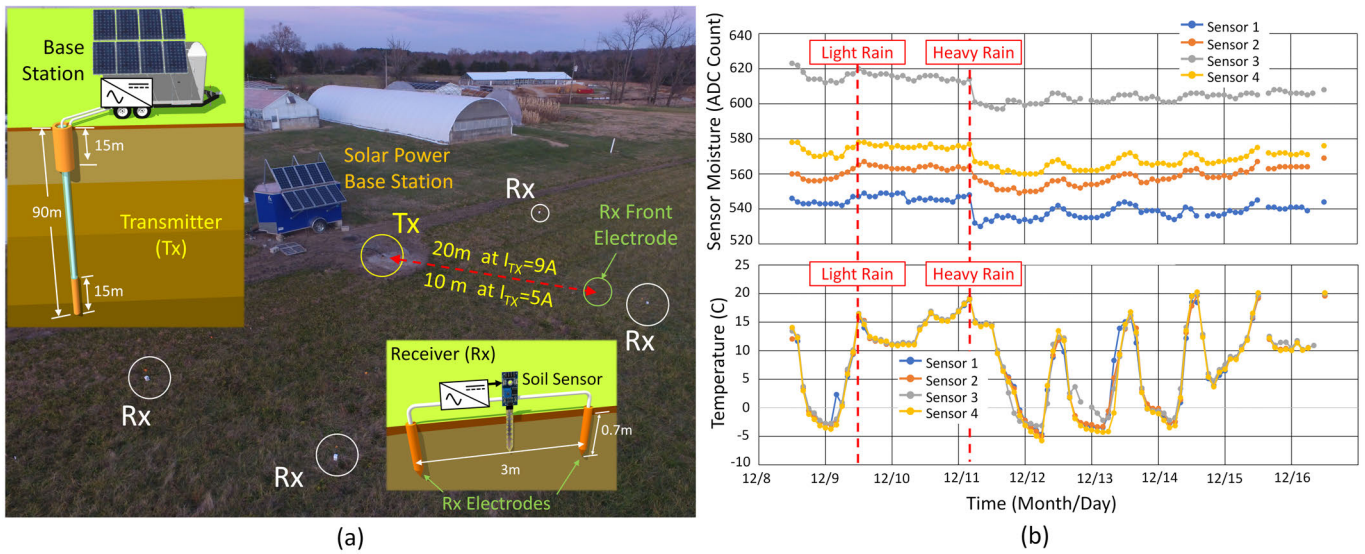

Fig. 8. **(a)** Photograph of IoT soil sensor modules deployed around the Tx. The modules had no batteries or large electric storage elements. They were powered directly from conduction currents transmitted through the soil **(b)** Plot of the soil sensor data powered continuously for one week during the month of December.

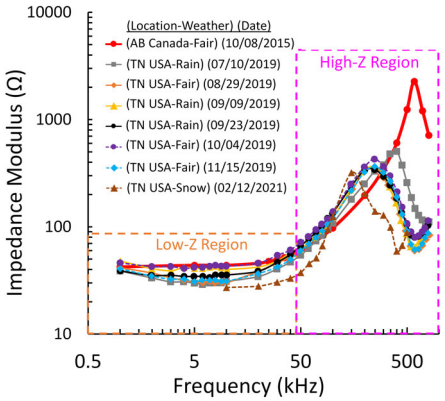

Fig. 9. Long-term impedance measurements over several months, weather conditions, and two different geographical locations. Variations from weather in the Low-Z region are significantly less than in the high-Z region.

the soil begins to function more like a dielectric. The peaks in this region are a parallel resonance that occurs with the Tx wiring and is observed to have very little energy output into the surrounding media. The high-Z region also fluctuates significantly with weather. The low-Z region not only exhibits the lowest Tx impedance, its fluctuation is between 30-50 Ω and is fairly consistent - even between locations that are 4,800km apart. It is important to note that both the US and Canadian locations were conducted on crop growing land - the soil thus had a high ion content making it better for plant growth, and consequently more electrically conductive. The data shows that the system, while dependent on soil parameters, is quite robust in the SLF to VLF frequency band. The data also indicates a tendency for the system impedance to be lower in more conductive soils with higher moisture, ion, or salinity content. This can be seen in Fig.9, when the soil moisture is higher, the Tx impedance tends to reduce – noting that snow in Tennessee is nearly always proceeded by rain, so soils are generally highly water saturated by the time snow fall occurs. The system is therefore expected to work better in locations of higher ion content (which is nearly all farming environments) and have lessened performance in drier soils.

Improving the efficiency of the system hinges on reducing the Z_{Tx} and Z_{Rx}. It was important to investigate the feasibility of altering the impedance values of at least the Tx. Literature indicates that the resistance of a soil-grounded electrical system can be significantly improved by adding multiple grounding rods [28], [29]. With this in mind, an experiment was conducted where the Tx impedance was measured using only the top electrode (well casing) (plotted in Fig. 10(a)) as the red (circle) trace entitled “no gnd rods”. The well casing in the inset illustration was also made red to match the data. The blue (triangle) trace was obtained by installing six 3m long grounding rods within a 3m radius around the casing such that all six rods and the casing formed the surface electrode. This new addition was made blue in the inset illustration to match the presented data. The simple addition of the grounding rods successfully reduced the Tx impedance as shown in the blue (triangle) trace of the figure.

The power required to operate 4 sensor modules was 0.8W (when transmitting data on 900MHz). The Z_{Rx} was measured at 250Ω for the 3m section between the Rx electrodes. Prior to installing the ground rods, it required a peak input power of 500W at 60Hz to operate the sensor network at a distance of 10m from the Tx. Note that this is the total system input power measured from the solar battery bank into the inverter that supplied power to the Tx. After adding the grounding rods, the same power delivery of 0.8W was achieved using 250W peak, a two fold improvement in efficiency with an addition of only 6 extra low-cost grounding rods. Experiments are underway to determine how low the Tx impedance can be

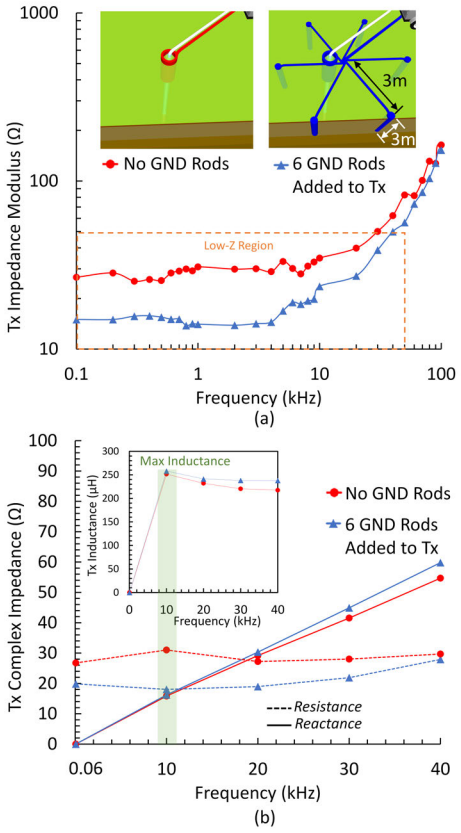

Fig. 10. (**a**) Measured Tx impedance using only the well casing (i.e. no ground rods) vs having a surface electrode composed of six grounding rods and the well casing. (**b**) Plots of the complex impedance with and without grounding rods. At higher frequencies, the inductive component of the Tx is more prevalent, having a peak inductance occuring at 10kHz.

made before the bottom electrode would need modification. In its present state, the TTS system is ideally suited for low power IoT applications with relatively infrequent measurements (such as agriculture). In the experiment, the field was energized for 1 minute every hour and shutdown for the remaining 59 minutes, leading to an average power of only one sixtieth of the peak power or $^{250}/_{60} = 4\,\text{W}$. The benefits of instrumenting a field and expending 10's of watts on average to know the locations of where to water, fertilize, or spray pesticides can make a significant impact on cost savings and the environment. Using renewable sources to power the TTS system also reduces the long-term cost of electricity.

The operation of sensor modules at drive frequencies higher than 60Hz is currently limited by our drive electronics. However, the low-Z frequency spectrum of the Tx can give insight into such operations. Fig. 10(b) shows that as the frequency increases, the Tx begins to function more like an inductor and less like a resistor; with a maximum inductance occurring at 10kHz. The addition of the grounding rods appeared to only affect the Tx resistance, not the reactance. This is important since an inductive Tx would not dissipate but store energy in its magnetic field every half cycle, allowing for resonant circuits to be utilized for possible range/efficiency improvements.

The theoretical model also predicts improved efficiency at higher drive frequencies. Using (8), the theoretically calculated transfer efficiency for a single sensor module, as a function of distance (r), is plotted in Fig. 11(a). The plot shows the response of reducing Z_{Tx} impedances at three different operating frequencies. Here, Z_{Rx} and R_L were kept the same as the experimental data (250Ω and 56Ω, respectively). While these theoretical plots of efficiency look promising, we are still in the process of validating Fig. 11(a), and will communicate such validations in future work. The full system efficiency for the proof-of-concept system, while presently low, are similar to values reported for MPT and laser based technologies. Yet unlike MPT/Lasers, the TTS system is not line-of-sight dependent and does not require the use of complex/expensive receivers. Moreover, the efficiency of the TTS system can be improved by lowering the impedance of the Tx and Rx, which is quite achievable via inexpensive grounding rods. A MPT/Laser system is instead limited by optical-electric conversion processes and beam directionality which has constraints both on safety and complexity/cost of the array.

Furthermore, there does not seem to be a limitation on the TTS transfer range according to the derived theory. Taking (19), a drive current of 200A at 60Hz is predicted to enable power transfer over 40-ha (100 acres) to sensors with a 3m Rx electrode separation (11). 40-ha is the approximate average farm size in the United States using statistical data from [30]. Close to the Tx, the step potential safety limit exceeds 25V between 1m. A 40m radius around the Tx would need to be restricted from access during operation. Beyond 40m, the step potential is low enough to walk freely. It is possible that the system may cause environmental effects/impacts. However, there has been no negative effects yet observed in the flora or fauna during the course of these studies. Some literature has shown that currents through soil can be beneficial to the growth of plants [31]. It was also discovered that telluric currents generated from a substation 0.8km away can be observed at the Tx [24]. Measured data shows the Tx receives approximately $5.6V_{Peak}$ from the substation. For a voltage of this magnitude to be measured at the Tx, it can be inferred from theoretical models that the magnitude seen at the substation must be quite large. Since this is an unintentional byproduct of a substation with flourishing trees and vegetation, it can be deduced that the effects on the environment are minimal. Moreover, if a substation can produce effects at such a distance unintended - the possibility of a designed TTS system achieving the same or better level of performance is encouraging.

V. Conclusion

A new LR-WPT technique was presented that utilizes conduction currents through soil to transmit power to sensing devices. A proof-of-concept prototype was constructed that successfully demonstrated power transfer to a small agricultural IoT network within a 20m radius. The energy transfer is not line-of-sight and simultaneously powers all sensors in the area; making it an ideal tool for agricultural IoT networks. A major benefit of the presented system is that each sensor module does not need an individual battery. Instead, batteries can be placed at a central location and the energy distributed radially around that location without wires.

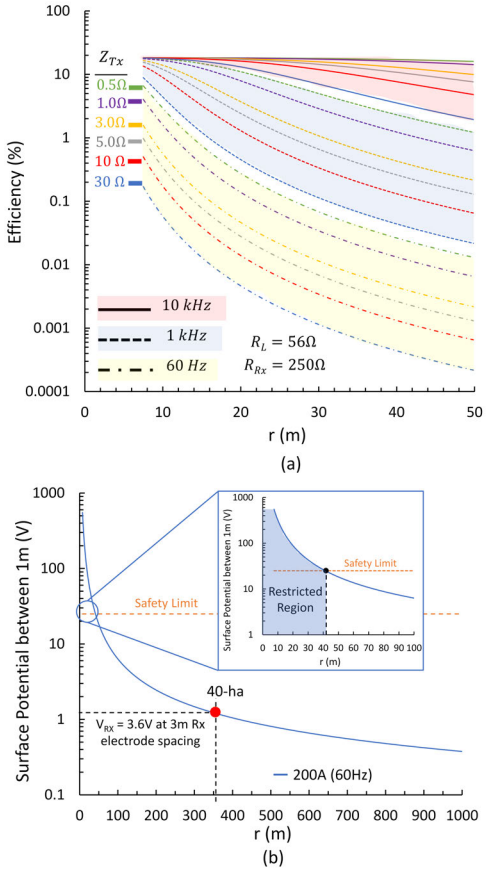

Fig. 11. (a) Calculation of efficiency vs range using (8), where u_e is calculated from (20), as Z_{Tx} is reduced from 30Ω to 0.5Ω. The highlighted areas indicate different operating frequencies. (b) Estimated drive current of 200A at 60Hz, using (19), needed to power sensor modules over a 40-ha (100 acre) area. Rx electrode separation is 2m to receive 5V.

This work has provided theory, simulation, scaling, and transfer parameters that quantify the operation of the TTS system. The power transfer range was found to be dependent on the injected Tx current while the efficiency was found to be dependent on the Tx and Rx bulk impedance. Increasing drive current while developing methods to lower the Tx/Rx impedance has the exciting *potential* to wirelessly power devices over great distances. This would revolutionize farm management and transform energy security as higher efficiency and power transfer is achieved. Future work will focus on the development of TTS communications in tandem with power, methods to reduce Tx impedance, and investigations into the effects of frequency and waveform shapes on the power transmission.

VI. Acknowledgment

This work was funded by the National Science Foundation Award Numbers 1841469 and 2226612, the Center for Energy Systems Research, and the Electrical and Computer Engineering Department at Tennessee Technological University, Cookeville, Tennessee, USA.

References

[1] H. Jabbar, Y. S. Song, and T. T. Jeong, "RF energy harvesting system and circuits for charging of mobile devices," *IEEE Transactions on Consumer Electronics*, vol. 56, no. 1, pp. 247–253, Feb. 2010, conference Name: IEEE Transactions on Consumer Electronics.

[2] B. Griffin and C. Detweiler, "Resonant wireless power transfer to ground sensors from a UAV," in *2012 IEEE International Conference on Robotics and Automation*, May 2012, pp. 2660–2665, iSSN: 1050-4729.

[3] M. T. Nguyen, C. V. Nguyen, L. H. Truong, A. M. Le, T. V. Quyen, A. Masaracchia, and K. A. Teague, "Electromagnetic Field Based WPT Technologies for UAVs: A Comprehensive Survey," *Electronics*, vol. 9, no. 3, p. 461, Mar. 2020, number: 3 Publisher: Multidisciplinary Digital Publishing Institute.

[4] J. M. Arteaga, P. D. Mitcheson, and E. M. Yeatman, "Development of a Fast-Charging Platform for Buried Sensors Using High Frequency IPT for Agricultural Applications," in *2022 IEEE Applied Power Electronics Conference and Exposition (APEC)*, Mar. 2022, pp. 1116–1121, iSSN: 2470-6647.

[5] Y. Pang, Y. Zhang, Y. Gu, M. Pan, Z. Han, and P. Li, "Efficient data collection for wireless rechargeable sensor clusters in Harsh terrains using UAVs," in *2014 IEEE Global Communications Conference*, Dec. 2014, pp. 234–239, iSSN: 1930-529X.

[6] M. Sansoy, A. S. Buttar, and R. Goyal, "Empowering Wireless Sensor Networks with RF Energy Harvesting," in *2020 7th International Conference on Signal Processing and Integrated Networks (SPIN)*, Feb. 2020, pp. 273–277, iSSN: 2688-769X.

[7] J. M. Arteaga, J. O'Keefe, D. E. Boyle, P. D. Mitcheson, and E. Yeatman, "Interrogation and Charging of Embedded Sensors by Autonomous Vehicles," in *2021 21st International Conference on Solid-State Sensors, Actuators and Microsystems (Transducers)*. Orlando, FL, USA: IEEE, Jun. 2021, pp. 296–299.

[8] C. Caillouet, T. Razafindralambo, and D. Zorbas, "Recharging wireless sensor networks using drones and wireless power transfer," in *2018 IEEE 29th Annual International Symposium on Personal, Indoor and Mobile Radio Communications (PIMRC)*, Sep. 2018, pp. 1136–1137, iSSN: 2166-9589.

[9] Z. W. Sim, "Radio Frequency Energy Harvesting for Embedded Sensor Networks in the Natural Environment," Apr. 2012, publisher: The University of Manchester, Manchester, UK.

[10] G. Indumathi and K. Karthika, "Rectenna design for RF energy harvesting in wireless sensor networks," in *2015 IEEE International Conference on Electrical, Computer and Communication Technologies (ICECCT)*, Mar. 2015, pp. 1–4.

[11] C. T. Rodenbeck, P. I. Jaffe, B. H. Strassner II, P. E. Hausgen, J. O. McSpadden, H. Kazemi, N. Shinohara, B. B. Tierney, C. B. DePuma, and A. P. Self, "Microwave and Millimeter Wave Power Beaming," *IEEE Journal of Microwaves*, vol. 1, no. 1, pp. 229–259, Jan. 2021, conference Name: IEEE Journal of Microwaves.

[12] X. Zhu, K. Jin, Q. Hui, W. Gong, and D. Mao, "Long-Range Wireless Microwave Power Transmission: A Review of Recent Progress," *IEEE Journal of Emerging and Selected Topics in Power Electronics*, vol. 9, no. 4, pp. 4932–4946, Aug. 2021, conference Name: IEEE Journal of Emerging and Selected Topics in Power Electronics.

[13] R. M. Dickinson, "Evaluation of a microwave high-power reception-conversion array for wireless power transmission," Tech. Rep. NASA-CR-145625, Sep. 1975, nTRS Author Affiliations: Jet Propulsion Lab., California Inst. of Tech. NTRS Document ID: 19760004119 NTRS Research Center: Legacy CDMS (CDMS). [Online]. Available: https://ntrs.nasa.gov/citations/19760004119

[14] A. Douyère, G. Pignolet, E. Rochefeuille, F. Alicalapa, J.-D. L. S. Luk, and J.-P. Chabriat, ""Grand Bassin" Case Study: An Original Proof-Of-Concept Prototype for Wireless Power Transportation," in *2018 IEEE Wireless Power Transfer Conference (WPTC)*, Jun. 2018, pp. 1–4, iSSN: 2573-7651.

[15] X. Yi, X. Chen, L. Zhou, S. Hao, B. Zhang, and X. Duan, "A Microwave Power Transmission Experiment Based on the Near-Field Focused Transmitter," *IEEE Antennas and Wireless Propagation Letters*, vol. 18, no. 6, pp. 1105–1108, Jun. 2019, conference Name: IEEE Antennas and Wireless Propagation Letters.

[16] "Ossia: Proven Wireless Power Technology You Can Use Today." [Online]. Available: https://www.ossia.com/

[17] "Emrod Energy | Long Range Wireless Power Transmission." [Online]. Available: https://emrod.energy/

[18] U. Raza and A. Salam, "Zenneck Waves in Decision Agriculture: An Empirical Verification and Application in EM-Based Underground Wireless Power Transfer," *Smart Cities*, vol. 3, no. 2, pp. 308–340,

Jun. 2020, number: 2 Publisher: Multidisciplinary Digital Publishing Institute. [Online]. Available: https://www.mdpi.com/2624-6511/3/2/17
[19] S. Bourgiotis, P. Frangos, S. Sautbekov, and M. Pshikov, "The Evaluation of an Asymptotic Solution to the Sommerfeld Radiation Problem Using an Efficient Method for the Calculation of Sommerfeld Integrals in the Spectral Domain," *Electronics*, vol. 10, no. 11, p. 1339, Jan. 2021, number: 11 Publisher: Multidisciplinary Digital Publishing Institute.
[20] K. Corum, J. Corum, and M. Miller, "Surface waves and the 'crucial' propagation experiment — The key to efficient wireless power delivery," in *2016 Texas Symposium on Wireless and Microwave Circuits and Systems (WMCS)*, Mar. 2016, pp. 1–4.
[21] "Contact Us – Viziv Technologies." [Online]. Available: https://vizivtechnologies.com/contact/
[22] C. A. Robinson, B. T. Nieman, R. Craven, M. E. Bima, and C. W. Van Neste, "Development of A Wireless Power Transmission System for Agriculture Sensor Devices," in *2020 IEEE International Conference on Big Data (Big Data)*. Atlanta, GA, USA: IEEE, Dec. 2020, pp. 2360–2364. [Online]. Available: https://ieeexplore.ieee.org/document/9377855/
[23] C. W. Van Neste, R. Hull, J. E. Hawk, A. Phani, M. J. Unsworth, and T. Thundat, "Electrical excitation of the local earth for resonant, wireless energy transfer," *Wireless Power Transfer*, vol. 3, no. 2, pp. 117–125, Sep. 2016, publisher: Cambridge University Press.
[24] B. T. Nieman, M. G. Pearce, C. S. Johnson, M. Tidwell, J. Whitehead, and C. W. Van Neste, "Thru-the-Soil Long Range Wireless Power Transfer," in *2022 Wireless Power Week (WPW)*, Jul. 2022, pp. 372–377.
[25] K. F. Lee, *Principles of Antenna Theory*. Wiley, Jan. 1984.
[26] M. Loewer, T. Günther, J. Igel, S. Kruschwitz, T. Martin, and N. Wagner, "Ultra-broad-band electrical spectroscopy of soils and sediments—a combined permittivity and conductivity model," *Geophysical Journal International*, vol. 210, no. 3, pp. 1360–1373, Sep. 2017. [Online]. Available: https://doi.org/10.1093/gji/ggx242
[27] T. Brooking, N. Janse van Rensburg, and R. Fourie, "The improved utilisation of existing rural networks with the use of intermediate voltage and single wire earth return systems," in *3D Africon Conference. Africon '92 Proceedings (Cat. No.92CH3215)*, Sep. 1992, pp. 228–234.
[28] S. D. Buba and W. F. W. Ahmad, "REDUCTION OF EARTH GRID RESISTANCE BY ADDITION OF EARTH RODS TO VARIOUS GRID CONFIGURATIONS," vol. 11, no. 7, p. 6, 2016.
[29] M. G. Unde and B. E. Kushare, "Cost effective design of grounding grid using ground rods — A case study," in *2012 IEEE Fifth Power India Conference*, Dec. 2012, pp. 1–6.
[30] R. A. Hoppe, J. M. MacDonald, and P. Korb, "Small Farms in the United States," *United States Department of Agriculture*, no. EIB-63.
[31] T. Okumura, Y. Muramoto, and N. Shimizu, "Influence of DC electric field on growth of daikon radish (Raphanus sativus)," *IEEE Transactions on Dielectrics and Electrical Insulation*, vol. 19, no. 6, pp. 2237–2241, Dec. 2012, conference Name: IEEE Transactions on Dielectrics and Electrical Insulation.

Brandon Nieman (Student Member, IEEE) was born in Winchester, Tennessee in 1997. He received his B.S. and M.S. in Electrical Engineering from Tennessee Tech University in 2020 and 2022, respectively. He is currently working at Dynetics Inc. in Huntsville, Alabama as an Electrical Engineer. His areas of interest include electromagnetics, communications, and embedded system design.

Christopher S. Johnson (Student Member, IEEE) was born in Columbia, Tennessee, in 1999. He is a graduate student pursing a Ph.D. degree in Electrical and Computer Engineering at Tennessee Tech University. He received his B.S. in Electrical and Computer Engineering from Tennessee Tech in 2022. His current research interests include power electronics, wireless power transfer, and electromagnetic field phenomena.

Matthew G. S. Pearce (Member, IEEE) was born in Dunedin, New Zealand, in 1992.

He received his B.E. (Hons.) and Ph.D. degrees in electrical and electronic engineering from The University of Auckland, Auckland, New Zealand, in 2014 and 2020, respectively.

His current research interests include power electronics, wireless power transfer, and electric transportation. He is currently employed as a Post Doctoral Researcher at the Center for Energy Systems Research, Tennessee Technological University, Cookeville, Tennessee, U.S.A.

Tyler Marcrum (Student Member, IEEE) is a graduate student pursuing a Ph.D. degree in the Electrical and Computer Engineering department at Tennessee Tech University. He is currently employed as a Research Assistant in the Center for Energy Systems Research at Tennessee Tech. He received his B.S. in Electrical Engineering with a concentration in mechatronics from Tennessee Tech in 2020. Mr. Marcruum's research interest include quasi-wireless robots with aerospace applications, impedance matching networks for resonant devices, and nontraditional communication systems for wireless power transfer applications.

M. Caleb Thorne was born in Columbia, TN in 1997. He currently lives in Cookeville, TN, and is expected to graduate with his B.S. Degree in Electrical Engineering from Tennessee Tech University in December 2022. His areas of interest include electromagnetics and power systems.

Carter Ashby is from Winchester, Tennessee. He currently lives in Cookeville, Tennessee, where he is working toward his B.S. in Electrical Engineering at Tennessee Tech University. His interests include power systems, electromagnetics, and embedded systems.

Charles W. van Neste (Senior Member, IEEE) was born in West Palm Beach, Florida in 1981. He received his B.S. and Ph.D. degrees in Electrical Engineering from Tennessee Tech University in 2004 and 2009 followed by a post doctoral fellowship at Oak Ridge National Laboratory in 2010.

From January 2011 to June 2017 he was a Research Associate at the University of Alberta in Canada. In 2017 he returned to the USA, and from 2017 until 2020 he was a Research Professor in the Center for Energy Systems Research at Tennessee Tech. He is currently an Assistant Professor working in the Electrical and Computer Engineering Department at Tennessee Tech where he teaches electromagnetics and continues to develop novel forms of energy transmission and generation. His research interests include wireless and quasi-wireless power transfer, power electronics, sensing, and instrumentation.

Dr. Van Neste is a member of the Society of Photo-Optical Instrumentation Engineers (SPIE) and is a Senior Member of the IEEE.